Subgrid Methods for Resolving Axial Heterogeneity in Planar Synthesis Solutions for the Boltzmann Transport Equation

Ph.D. Defense

Aaron M. Graham

July 20, 2017

- Predicting the neutron flux distribution is crucial for reactor analysis
- The flux distribution determines the power distribution, which has important ramifications for design and operation
    - Economically, efficient fuel loading patterns and prevention of fuel failures are determined largely by the power distribution
    - The power distribution also drives safety constraints for both steady-state and transient operation, including accident scenarios
- These requirements demand a high degree of accuracy from the codes used in reactor analysis

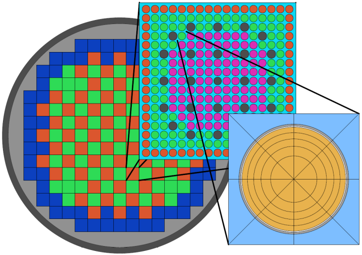

- Reactor analysis has traditionally used a two-step approach
  - Lattice calculations to generate homogenized cross sections
  - Nodal diffusion methods to solve global problem with homogenized cross sections
- Recent increases in computing power have generated interest in direct, whole-core transport calculations
  - Monte Carlo
  - Deterministic 3D transport
  - Planar Synthesis Methods: 2D/1D and 2D/3D

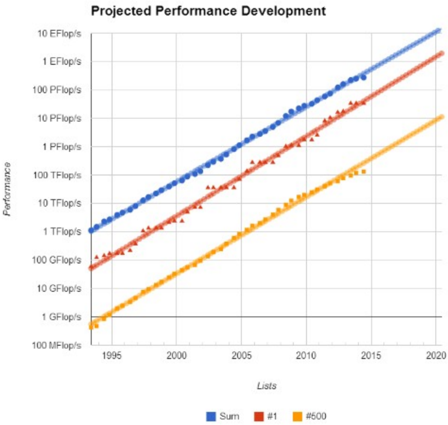

- Monte Carlo
  - Randomly samples cross sections to simulate the life of individual neutrons
  - Simulating many neutrons can be used to describe average behavior of neutrons throughout reactor
  - Prohibitively slow for large problems due to statistical uncertainties
- Deterministic 3D transport
  - Numerical methods are used to solve the transport equation in 3D
  - Accurate solutions can be obtained
  - Solving the transport equation can be too expensive for large problems
- Planar Synthesis Methods
  - Problem is decomposed into a stack of 2D planes, each assumed to be axially constant
  - 2D transport equation is solved for each 2D plane, then coupled using a fast 1D solver (2D/1D) or 3D solver (2D/3D)
  - Preserves much of the accuracy of 3D transport, but runs much faster

Rod Cusping

- Planar synthesis methods require planes to be axially homogeneous
- If any axial heterogeneities are present in the plane, they must be homogenized axially
- Volume homogenization is used since flux distribution is not yet known
- Control rods are strong neutron absorbers, causing the most severe homogenization errors
- Errors caused by rods partially inserted in a plane are called "rod cusping"

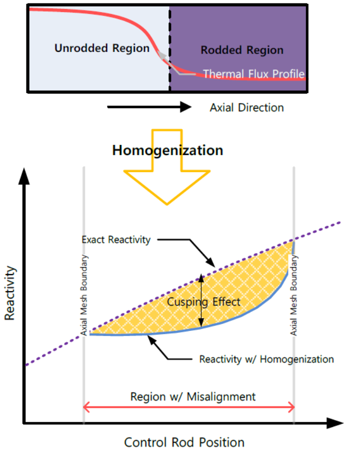

- Planar synthesis methods are faster than 3D transport, but still computationally expensive
- To make these methods useful practically, runtimes need to be decreased
  - Algorithm and methods improvements
  - Reduction in number of planes
- Subgrid methods can be used to maintain accuracy with fewer planes by loosening requirement that planes be axially homogeneous
  - Needs to be able to capture local effects of various reactor components
  - Should be able to be applied to a variety of situations
  - Cheaper than using more planes
- Three new methods developed to accomplish two goals:
  - Significant reduction in errors caused by rod cusping, the most severe axial heterogeneity for planar synthesis methods
  - Reduce the runtime of the 2D/1D code MPACT by using fewer planes

Boltzmann Transport Equation

$$
\begin{aligned}
&\frac{1}{v}\frac{\partial \varphi}{\partial t} + \boldsymbol{\Omega}\cdot\boldsymbol{\nabla}\varphi + \Sigma_t\left(\boldsymbol{x},E,t\right)\varphi\left(\boldsymbol{x},E,\boldsymbol{\Omega},t\right) \\
&\quad = \frac{1}{4\pi}\int\limits_{0}^{\infty}\int\limits_{4\pi}\Sigma_s\left(\boldsymbol{x},E'\to E,\boldsymbol{\Omega}'\to\boldsymbol{\Omega}\right)\varphi\left(\boldsymbol{x},E',\boldsymbol{\Omega}'\right)d\Omega' dE' \\
&\qquad + \frac{\chi_p\left(\boldsymbol{x},E\right)}{4\pi}\int\limits_{0}^{\infty}\int\limits_{4\pi}\left(1-\beta\left(\boldsymbol{x},E'\right)\right)\nu\Sigma_f\left(\boldsymbol{x},E',t\right)\varphi\left(\boldsymbol{x},E',\boldsymbol{\Omega}',t\right)d\Omega' dE' \\
&\qquad + \sum_{j=1}^{N_d}\frac{\chi_{d,j}\left(\boldsymbol{x},E\right)}{4\pi}\lambda_j C_j\left(\boldsymbol{x},t\right) + Q\left(\boldsymbol{x},E,\boldsymbol{\Omega},t\right)
\end{aligned}
$$

$$
\varphi\left(\boldsymbol{x}_b,E,\boldsymbol{\Omega},t\right) = \varphi^b\left(\boldsymbol{x}_b,E,\boldsymbol{\Omega},t\right)\ , \quad \boldsymbol{\Omega}\cdot\boldsymbol{n} < 0
$$

Boltzmann Transport Equation

- Transport equation is continuous in space, time, energy and angle
- For this work, only the steady-state eigenvalue form of the equation is considered
- Multigroup approximation is used to discretize in energy
- Angles are discretized, using an angular quadrature to integrate the angular flux φ

Steady-State Transport Equation

$$
\begin{aligned}
&\mathbf{\Omega}_n \cdot \nabla \varphi_{g,n} + \Sigma_{t,g}\left(\boldsymbol{x}\right) \varphi_{g,n}\left(\boldsymbol{x}\right) \\
&\quad = \frac{1}{4\pi} \sum_{g'=1}^{G} \sum_{n'=1}^{N} \Sigma_{g' \to g, n' \to n}\left(\boldsymbol{x}\right) \varphi_{g',n'}\left(\boldsymbol{x}\right) w_{n'} \\
&\qquad + \frac{1}{k_{eff}} \frac{\chi_g}{4\pi} \sum_{g'=1}^{G} \sum_{n'=1}^{N} \nu \Sigma_{f,g'}\left(\boldsymbol{x}\right) \varphi_{g',n'}\left(\boldsymbol{x}\right) w_{n'}
\end{aligned}
$$

$$
\varphi_{g,n}\left(\boldsymbol{x}_b\right) = \varphi_g^b\left(\boldsymbol{x}_b, \mathbf{\Omega}_n\right) \;, \quad \mathbf{\Omega}_n \cdot \boldsymbol{n} < 0
$$

- Calculations discussed here use transport-corrected isotropic scattering (TCP_0) to simplify the scattering source

Diffusion Approximation

- Assumes linearly anisotropic angular flux and a simple relationship between scalar flux ϕ and current J

$$\varphi_g(\boldsymbol{x},\boldsymbol{\Omega}) \approx \frac{1}{4\pi}(\phi_g(\boldsymbol{x}) + 3\boldsymbol{\Omega}\cdot\boldsymbol{J}_g(\boldsymbol{x}))$$

$$\phi_g(x) = \int_{4\pi} \psi_g(\boldsymbol{x},\boldsymbol{\Omega}) d\Omega$$

$$\boldsymbol{J}(\boldsymbol{x}) \approx -\boldsymbol{D}(\boldsymbol{x})\boldsymbol{\nabla}\phi(x)$$

$$\boldsymbol{D}(\boldsymbol{x}) = \frac{1}{3}(\boldsymbol{\Sigma}_{tr,g}(\boldsymbol{x}))^{-1}$$

- Eliminates angle dependence, simplifies streaming and scattering source terms

$$-\boldsymbol{\nabla}\cdot\boldsymbol{D}_g(\boldsymbol{x})\boldsymbol{\nabla}\phi(\boldsymbol{x}) + \Sigma_{t,g}(\boldsymbol{x})\phi_g(\boldsymbol{x}) = \sum_{g'=1}^{G} \Sigma_{s0,g'\to g}(\boldsymbol{x})\phi_{g'}(\boldsymbol{x}) + \frac{1}{k_{eff}}\frac{\chi_g}{4\pi}\sum_{g'=1}^{G} \nu\Sigma_{f,g'}(\boldsymbol{x})\phi_{g'}(\boldsymbol{x}) + Q_g(\boldsymbol{x})$$

$$\frac{1}{4}\phi_g(\boldsymbol{x}_b) + \frac{\boldsymbol{D}_g(x_b)}{2}\cdot\boldsymbol{\nabla}\phi(\boldsymbol{x}_b) = J_g^-(\boldsymbol{x}_b)$$

Background

- 2D/1D method was developed by researchers at Korea Atomic Energy Research Institute (KAERI) [1, 2, 3]
- Newer 2D/1D code MPACT, jointly developed by University of Michigan and Oak Ridge National Laboratory, is used for this work [4]

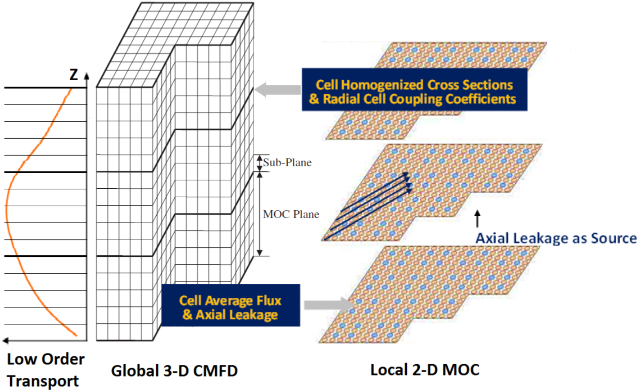

Radial Equations

- Average transport equation axially from $z_{k-\frac{1}{2}}$ to $z_{k+\frac{1}{2}}$
- Assume cross sections are axially constant in region of integration

$$\Omega_x \frac{\partial \psi_g^Z}{\partial x} + \Omega_y \frac{\partial \psi_g^Z}{\partial y} + \Sigma_{tr,g}(x,y)\,\psi_g^Z(x,y,\boldsymbol{\Omega}) = q_g^Z(x,y,\boldsymbol{\Omega}) + L_g^Z(x,y,\Omega_z)$$

$$q_g^Z(x,y,\boldsymbol{\Omega}) = \frac{1}{4\pi}\sum_{g'=1}^{G}\int_{4\pi} \Sigma_{s,g'\to g}^Z(x,y,\boldsymbol{\Omega}'\cdot\boldsymbol{\Omega})\,\psi_{g'}^Z(x,y,\boldsymbol{\Omega}')\,d\Omega' + \frac{1}{k_{eff}}\frac{\chi_g^Z}{4\pi}\sum_{g'=1}^{G}\int_{4\pi}\nu\Sigma_{f,g'}^Z(x,y)\,\psi_{g'}^Z(x,y,\boldsymbol{\Omega}')\,d\Omega' + \frac{Q_g^Z(x,y)}{4\pi}$$

$$L_g^Z(x,y,\Omega_z) = \frac{\Omega_z}{\Delta z_k}\left(\psi_{g,z_{k-\frac{1}{2}}} - \psi_{g,z_{k+\frac{1}{2}}}\right) \approx \frac{J_{g,z_{k-\frac{1}{2}}} - J_{g,z_{k+\frac{1}{2}}}}{4\pi\Delta z_k}$$

Axial Equations

- Average transport equation over x from $x_{i-\frac{1}{2}}$ to $x_{i+\frac{1}{2}}$ and over y from $y_{j-\frac{1}{2}}$ to $y_{j+\frac{1}{2}}$
- Assume cross sections are radially constant in region of integration

$$\Omega_z \frac{\partial \psi_g^{XY}}{\partial z} + \Sigma_{tr,g}^{XY}(z)\,\psi_g^{XY}(z,\boldsymbol{\Omega}) = q_g^{XY}(z,\boldsymbol{\Omega}) + L_g^{XY}(z,\Omega_x,\Omega_y)$$

$$L_g^{XY}(z,\Omega_x,\Omega_y) \approx \frac{J_{g,x_{i-\frac{1}{2}},y_j} - J_{g,x_{i+\frac{1}{2}},y_j}}{4\pi\Delta x_i} + \frac{J_{g,x_i,y_{j-\frac{1}{2}}} - J_{g,x_i,y_{j+\frac{1}{2}}}}{4\pi\Delta y_j}$$

Calculation Flow

- 3D Coarse Mesh Finite Difference (CMFD) [5]
  - Determines global flux shape to scale fine mesh solution
  - Calculates radial currents for 1D axial solver
- 1D NEM-P_3 [6, 7]
  - Calculates improved axial currents for 2D solver
- 2D Method of Characteristics (MOC) [8, 9]
  - Solves for fine mesh scalar flux
  - Calculates updated radial currents for CMFD calculation

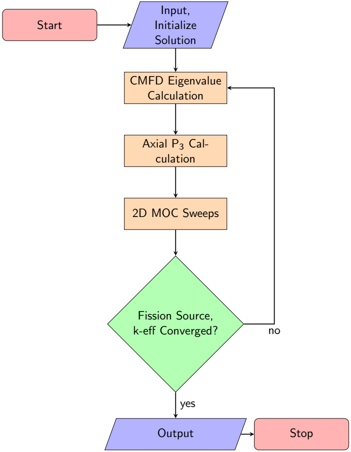

3D CMFD

- Diffusion-based acceleration performed on coarse mesh
- $\hat{D}$ coupling coefficients enforce consistency between diffusion and transport solutions

$$\hat{D}_{g,s}=\frac{J_{g,s}^{trans,k-1}+\tilde{D}_{g,s}\left(\phi_{g,p}^{diff,k}-\phi_{g,m}^{diff,k}\right)}{\left(\phi_{g,p}^{trans,k}+\phi_{g,m}^{diff,k}\right)}$$

- Coarse mesh solution projected onto the fine mesh, preserving MOC radial shape and CMFD volume-averaged flux

$$\phi_{g,j}^{trans,k}=\frac{\phi_{g,i}^{diff,k}}{\phi_{g,i}^{diff,k-1}}\phi_{g,j}^{trans,k-1}$$

- Subplane scheme is used to capture subplane axial flux shapes

1D NEM-P_3

- P_3 [6] used to handle angular shape
  - Angular flux expanded in terms of Legendre polynomials:

$$\varphi(x,\mu) \approxeq \sum_{n=0}^{N} \frac{2n+1}{2} \varphi_n(x) P_n(\mu)$$

$$\Sigma_s\left(x,\mu,\mu'\right) = \sum_{n=0}^{N} \frac{2n+1}{2} P_n(\mu) P_n\left(\mu'\right) \Sigma_{s,n}(x)$$

  - Two diffusion-like equations

$$-\boldsymbol{\nabla}\cdot D_{0,g}(\boldsymbol{x})\boldsymbol{\nabla}\Phi_{0,g}(\boldsymbol{x}) + [\Sigma_{tr,g}(\boldsymbol{x}) - \Sigma_{s0,g}(\boldsymbol{x})]\Phi_{0,g}(\boldsymbol{x}) = Q_g(\boldsymbol{x}) + 2[\Sigma_{tr,g}(\boldsymbol{x}) - \Sigma_{s0,g}(\boldsymbol{x})]\Phi_{2,g}(\boldsymbol{x})$$

$$\begin{aligned} -\boldsymbol{\nabla}\cdot D_{2,g}(\boldsymbol{x})\boldsymbol{\nabla}\Phi_{2,g}(\boldsymbol{x}) + [\Sigma_{tr,g}(\boldsymbol{x}) - \Sigma_{s2,g}(\boldsymbol{x})]\Phi_{2,g}(\boldsymbol{x}) \\ = \frac{2}{5}\{[\Sigma_{tr,g}(\boldsymbol{x}) - \Sigma_{s0,g}(\boldsymbol{x})][\Phi_{0,g}(\boldsymbol{x}) - 2\Phi_{2,g}(\boldsymbol{x})] - Q_g(\boldsymbol{x})\} \end{aligned}$$

  - Iterating between these equations gives solution for Φ_0 and Φ_2, which can be used to solve for φ_0 and φ_2:

$$\varphi_0(x) = \Phi_0(x) - 2\Phi_2(x) \;, \quad \varphi_2(x) = \Phi_2(x)$$

1D NEM-P_3

- The Nodal Expansion Method (NEM) [7] used to handle spatial shape
  - Expand source and flux as quadratic and quartic polynomials:

$$Q(\xi)=\sum_{i=0}^{2} q_i P_i(\xi) \ , \quad \phi(\xi)=\sum_{i=0}^{4} \phi_i P_i(\xi)$$

  - 3 moment-balance and 2 continuity equations to solve for 5 flux coefficients:

$$\int_{-1}^{1} P_n(\xi)\left(-\frac{D}{h^2}\frac{d^2}{d\xi^2}\phi(\xi)+\Sigma_r\phi(\xi)-Q(\xi)\right)d\xi=0,\ \ n=0,1,2$$

$$\phi_L(1)=\phi_R(-1) \ , \quad J_L(1)=J_R(-1)$$

  - Applying this method to both P_3 equations gives a system of 10 equations for each group and each node

2D MOC

- Solve along a specific direction Ω_n to reduce the problem from a PDE to an ODE that can be solved analytically

$$\frac{\partial \psi_{g,n}}{\partial s} + \Sigma_{t,g}(\boldsymbol{r}_0 + s\boldsymbol{\Omega}_n)\psi_{g,n}(\boldsymbol{r}_0 + s\boldsymbol{\Omega}_n) = q_{g,n}(\boldsymbol{r}_0 + s\boldsymbol{\Omega}_n)$$

$$\begin{aligned} \psi_{g,n}(\boldsymbol{r}_0 + s\boldsymbol{\Omega}_n) = &\psi_{g,n}(\boldsymbol{r}_0) \exp\left(-\int_0^s \Sigma_{t,g}(\boldsymbol{r}_0 + s'\boldsymbol{\Omega}_n) ds'\right) \\ &+ \int_0^s q_{g,n}(\boldsymbol{r}_0 + s'\boldsymbol{\Omega}_n) \exp\left(-\int_0^{s'} \Sigma_{t,g}(\boldsymbol{r}_0 + s''\boldsymbol{\Omega}_n) ds''\right) ds' \end{aligned}$$

- Assume flat source, cross section along track with length L_j and spacing δx

$$\begin{aligned} \psi^{out}_{g,i,n,j} &= \psi^{in}_{g,i,n,j} e^{-\Sigma_{t,g,i} L_j} + \frac{q_{g,i,n}}{\Sigma_{t,g,i}}\left(1 - e^{-\Sigma_{t,g,i} L_j}\right) \\ \overline{\psi}_{g,i,n,j} &= \frac{q_{g,n,i}}{\Sigma_{t,g,i}} + \frac{1 - e^{-\Sigma_{t,g,i} L_j}}{L_j \Sigma_{t,g,i}}\left(\psi^{in}_{g,i,n,j} - \frac{q_{g,n,i}}{\Sigma_{t,g,i}}\right) \\ \overline{\psi}_{g,i,n} &= \frac{\sum_j \overline{\psi}_{g,i,n,j} \delta x L_j}{\sum_j \delta x L_j} \end{aligned}$$

2D MOC

- Perform ray tracing and store segment information up front
- Set up scattering, fission, and axial transverse leakage sources
- Solve each long ray one at a time
    - Incoming angular flux at each end of long ray is known from boundary conditions
    - Outgoing angular flux for each segment is used as incoming for subsequent segments
    - Region-wise scalar flux and surface currents are tallied as each long ray is swept

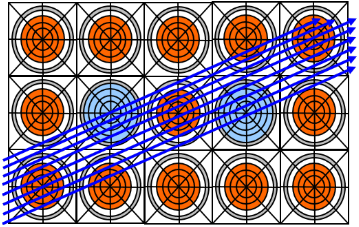

Rod Cusping

- Planar synthesis methods require planes to be axially homogeneous
- Control rods often do not align with plane boundaries, requiring rod and moderator to be homogenized
- Volume homogenization preserves material volume/mass, but not reaction rates; solution is unknown, but required for proper homogenization
- Two approaches to prevent rod cusping:
  - Refine mesh to align with all control rod positions
  - Decusping method to improve homogenization

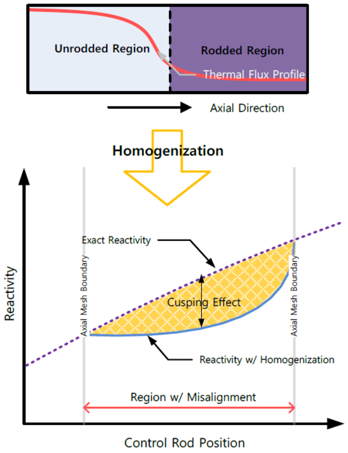

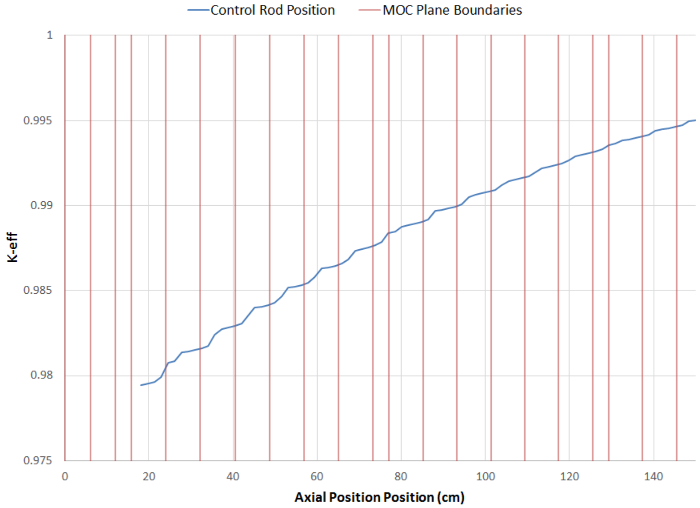

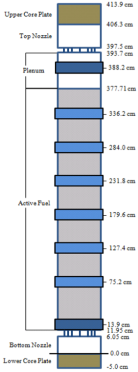

2.1	2.6 20 PY	2.1
2.6 20 PY	2.1 RCCA	2.6 20 PY
2.1	2.6 20 PY	2.1

2D/1D Decusping Methods

- Neighbor Spectral Index Method - CRX-2K [10]
  - Spectral index is defined as the ratio of the fast flux to the thermal flux
  - Spectral index is used in top and bottom neighbor nodes to estimate partially rodded node flux profile
  - This estimate is used to update cross sections each iteration
- nTRACER Method [11]
  - Solves local problem to generate CMFD constants
  - Performs CMFD calculations on fine mesh to obtain axial flux profiles
  - Uses axial flux profiles during full core calculation to homogenize cross sections
- Approximate Flux Weighting Method [12]
  - Originally developed for nodal methods, but also implemented in nTRACER [13]
  - Assumes that in partially rodded node, rodded flux is similar to node above and unrodded flux is similar to node below
  - Assumption allows the partially rodded node cross section to be updated easily during iteration

Methods Shortcomings

- Extensive research has been done on decusping methods, primarily for nodal codes
- Several methods have been developed for 2D/1D codes
  - Some methods involved coarse approximations with limited accuracy
  - Others required expensive additional calculations that increased runtime of the code significantly
- New methods need to improve on prior ones by providing more accurate solutions without significantly slowing down calculations

Polynomial Decusping

- Rodded 3×3 assembly case used to generate correction factors based on rod position
  - One set of calculations performed with refined mesh to eliminate cusping effects
  - Second set done with coarse mesh
  - Percent change in k_{eff} plotted against percent change in volume fraction for each set of calculations
  - Difference in curves used to reduce volume fraction during rod homogenization to reduce cusping effects
- Sixth order polynomial curves generated for AIC, B_4C, and tungsten rods

Polynomial Decusping

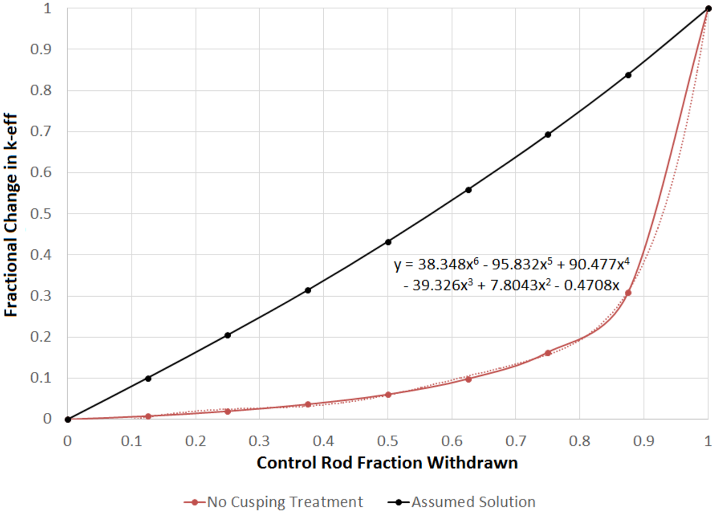

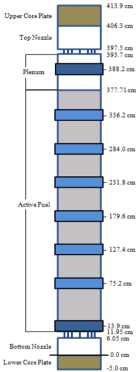

2.1	2.6 20 PY	2.1
2.6 20 PY	2.1 RCCA	2.6 20 PY
2.1	2.6 20 PY	2.1

Subplane Collision Probabilities

- Modifications made to subplane scheme [14, 15] to treat axial effects of rod cusping
  - Homogenization still uses MOC flux, but with heterogeneous rodded or unrodded cross sections
  - Projection rehomogenizes cross sections in partially rodded nodes after CMFD calculation

$$\overline{\Sigma_i} = \frac{\phi^R_{rad,i}\phi^R_{ax,i}\Sigma^R_i h^R + \phi^U_{rad,i}\phi^U_{ax,i}\Sigma^U_i h^U}{\phi^R_{rad,i}\phi^R_{ax,i}h^R + \phi^U_{rad,i}\phi^U_{ax,i}h^U}$$

Subplane Collision Probabilities

- Sub-plane modifications only capture axial effects
  - MOC uses homogenized cross section
  - Radial shape does not accurately reflect either region
- 1D collision probabilities (CP) introduced to generate radial shapes
  - Generates radial flux profile for rodded and unrodded region
  - Radial profiles used in CMFD homogenization
  - Fast calculation

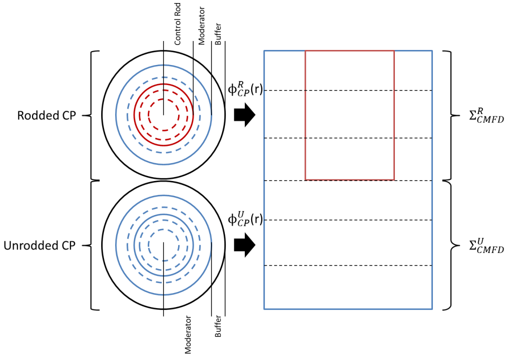

Subray Method of Characteristics

- Other methods do not correctly address the MOC calculation
  - Homogenized cross sections are still used for 2D MOC
  - Flux shape from MOC does not accurately represent rodded or unrodded flux
- To improve MOC solutions, heterogeneous cross sections and sources must be accounted for
- MOC rays can be split into subrays in the vicinity of partially rodded regions
- MOC solution along subrays exponentially converges to $\frac{q}{\Sigma_t}$, allowing subrays to be recombined once axial shape of q flattens sufficiently

Subray Method of Characteristics

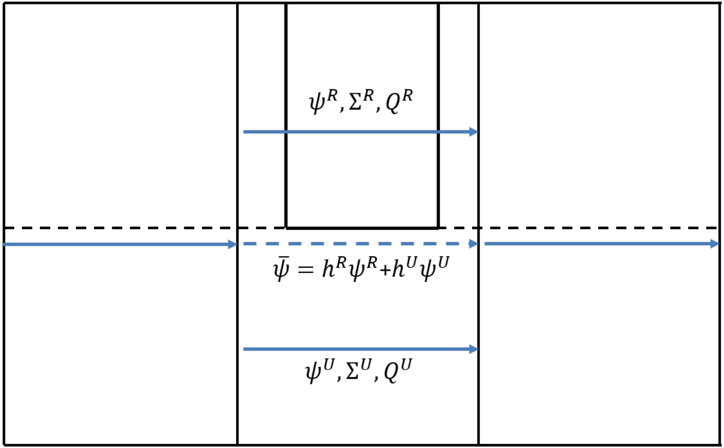

Subray Method of Characteristics

- Many modifications were required to enable subray MOC in MPACT:
  - Fluxes, cross sections, and sources are stored for subregions that subrays pass through
  - New MOC sweeper was developed that duplicates long rays using axial volume fractions to average rays together
  - CMFD projection is used to calculate subregion fluxes and generate subregion sources
  - Subplane CMFD/P_3 results are used to calculate axial TL sources in subregions
  - Option was added to control how far away from rod subray continues to be used

Subray Method of Characteristics

- Subray is used in the entire pin cell with the partially inserted control rod
- To capture farther reaching effects of the rod, subray can also be used in neighboring pin cells:
    - Subray-0 (Red)
    - Subray-1 (Blue)
    - Subray-2 (Green)
    - Subray-3 (White)
- Calculations become more expensive as more subrays are used, but accuracy should improve

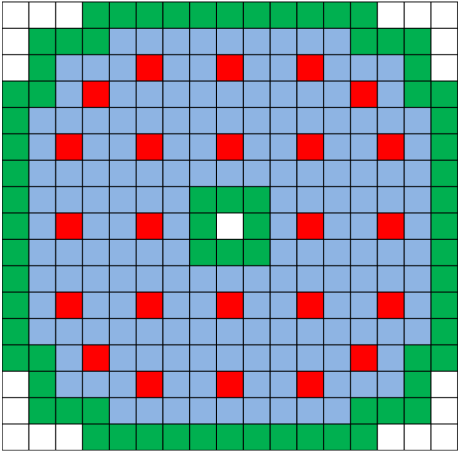

- VERA Progression Problems [16]
  - Series of 10 benchmark problems based on Watts Bar Unit 1 Pressurized Water Reactor (PWR)
  - Problems 4 and 5 were used to test polynomial and subplane CP methods
  - Subray MOC was not used on these problems due to cross sections shielding requirements
- C5G7 Benchmark Problems [17, 18]
  - Benchmark problem with UO_2 and MOX fuels
  - 7 energy groups
  - Various C5G7 configurations were used to test subray MOC and compare it to subplane CP

Problem Description

- Center 3x3 assembly cluster in Watts Bar Unit 1
- Heterogeneous AIC control rod with stainless steel tip and B_4C follower
- All simulations used 1 core per plane

2.1	2.6 20 PY	2.1
2.6 20 PY	2.1 RCCA	2.6 20 PY
2.1	2.6 20 PY	2.1

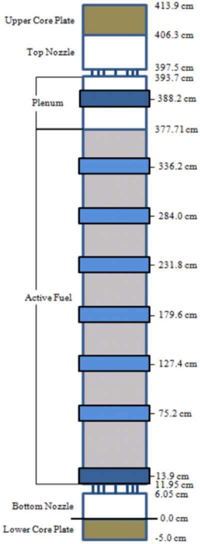

Test Procedures

- Differential rod worth curves were generated with coarse mesh using each decusping method
- Comparison of curves shows effectiveness of decusping methods as rod is withdrawn through core
- KENO-VI was used to calculate reference solutions at 10% intervals
    - 500 inactive generations
    - 10,000 active generations
    - 5×10^6 particles per generation

Differential Rod Worth Curve

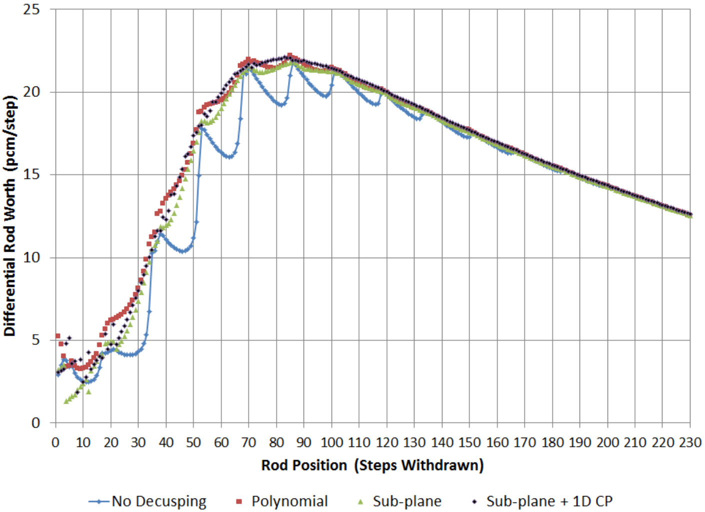

KENO-VI Comparisons

Cases	Decusping Method	k_{eff} Difference	Pin Power Difference RMS	Pin Power Difference Max
Average	None	−17.7	4.833%	23.037%
	Polynomial	35.5	1.365%	8.003%
	Subplane	35.5	0.940%	4.210%
	Subplane + CP	41.5	0.730%	3.069%
Worst – 20%	None	−174.5	14.893%	63.700%
	Polynomial	15.4	3.492%	25.145%
	Subplane	11.1	2.089%	10.096%
	Subplane + CP	47.4	1.143%	4.534%
Fully Withdrawn	–	40.1	0.242%	0.824%

- 10,000 active generations, 5×10^6 particles per generation
- Maximum k_{eff} uncertainty is 0.6 pcm
- Maximum pin power uncertainty anywhere is less than 0.002

Problem Description and Test Procedures

- Bank D inserted to 257.9 cm, other banks all out
- 57 planes for tests and 58 for reference, 16 cores per plane
- Decusping methods compared with fine mesh solution

	H	G	F	E	D	C	B	A
8	2.1	2.6 20	2.1	2.6 20	2.1	2.6 20	2.1	3.1 12
9	2.6 20	2.1	2.6 24	2.1	2.6 20	2.1	3.1 24	3.1
10	2.1	2.6 24	2.1	2.6 20	2.1	2.6 16	2.1	3.1 8
11	2.6 20	2.1	2.6 20	2.1	2.6 20	2.1	3.1 16	3.1
12	2.1	2.6 20	2.1	2.6 20	2.6	2.6 24	3.1	
13	2.6 20	2.1	2.6 16	2.1	2.6 24	3.1 12	3.1	
14	2.1	3.1 24	2.1	3.1 16	3.1	3.1		
15	3.1 12	3.1	3.1 8	3.1				

Enrichment
Number of Pyrex Rods

	H	G	F	E	D	C	B	A
8	D		A		D		C	
9						SB		
10	A		C				B	
11				A		SC		
12	D				D		SA	
13		SB		SD				
14	C		B		SA			
15								

Problem 5 Results

Case	k_{eff} Difference (pcm)	Pin Power Differences RMS	Max	2D/1D Iterations	Runtime (Core-Hours)
Reference	–	–	–	13	361.7
No Treatment	-22	6.90%	30.55%	13	410.7
Polynomial	-5	1.15%	4.85%	13	373.7
Subplane	-5	2.09%	10.20%	13	399.0
Subplane + CP	-1	0.50%	2.74%	13	425.6

- Maximum error for each comparison occurs in pins neighboring the partially rodded pin cell

Problem Description

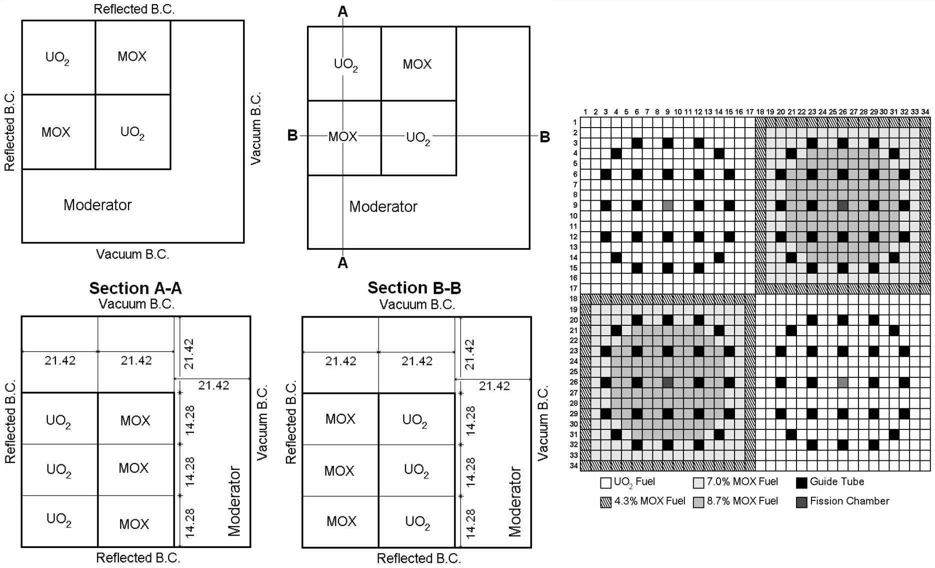

Test Procedure

- Three different C5G7 problems were simulated: 2D core, 3D assembly, and 3D core
- Rod was withdrawn through each problem in 1.428 cm increments for subray MOC and subplane methods
- k_{eff} and 3D pin power comparisons were made against a fine mesh reference solution at each position

2D Core Results

Rod Position	Reference k_{eff}	Subray-0 k_{eff}	Subray-0 Pin Powers RMS	Subray-0 Pin Powers Max	Subray-1 k_{eff}	Subray-1 Pin Powers RMS	Subray-1 Pin Powers Max	Subray-2 k_{eff}	Subray-2 Pin Powers RMS	Subray-2 Pin Powers Max	Subray-3 k_{eff}	Subray-3 Pin Powers RMS	Subray-3 Pin Powers Max
1*	1.06839	-15	0.10%	0.29%	-15	0.10%	0.29%	-15	0.10%	0.29%	-15	0.10%	0.29%
2	1.07746	-33	0.22%	0.67%	-34	0.22%	0.68%	-34	0.22%	0.67%	-34	0.22%	0.67%
3	1.08777	-53	0.32%	1.03%	-56	0.34%	1.07%	-55	0.34%	1.06%	-55	0.34%	1.06%
4	1.09919	-72	0.41%	1.34%	-78	0.45%	1.45%	-78	0.45%	1.44%	-78	0.45%	1.44%
5	1.11160	-89	0.46%	1.53%	-99	0.51%	1.69%	-98	0.50%	1.66%	-98	0.50%	1.66%
6	1.12495	-102	0.49%	1.66%	-115	0.55%	1.83%	-115	0.54%	1.82%	-115	0.54%	1.81%
7	1.13925	-112	0.49%	1.70%	-127	0.55%	1.88%	-126	0.55%	1.87%	-126	0.55%	1.86%
8	1.15469	-117	0.47%	1.65%	-133	0.53%	1.83%	-132	0.53%	1.81%	-132	0.52%	1.81%
9*	1.17190	-117	0.43%	1.50%	-127	0.46%	1.61%	-126	0.46%	1.60%	-126	0.46%	1.60%
Average	–	**79**	**0.38%**	**1.26%**	**87**	**0.41%**	**1.37%**	**87**	**0.41%**	**1.36%**	**87**	**0.41%**	**1.36%**

- Superscript * denotes cases run with axial diffusion instead of P_3

2D Core Results

Rod Position	Reference k_{eff}	Subray-0 k_{eff}	Subray-0 Pin Powers RMS	Subray-0 Pin Powers Max	None k_{eff}	None Pin Powers RMS	None Pin Powers Max	Subplane k_{eff}	Subplane Pin Powers RMS	Subplane Pin Powers Max	Subplane + CP k_{eff}	Subplane + CP Pin Powers RMS	Subplane + CP Pin Powers Max
1*	1.06839	-15	0.10%	0.29%	-286	1.73 %	4.47 %	-87	0.52%	1.35%	-169	0.99%	2.46%
2	1.07746	-33	0.22%	0.67%	-811	4.75 %	12.70%	-198	1.13%	3.06%	-174	0.97%	2.57%
3	1.08777	-53	0.32%	1.03%	-1369	7.71 %	21.30%	-290	1.56%	4.42%	-181	0.97%	2.70%
4	1.09919	-72	0.41%	1.34%	-1918	10.33%	29.42%	-360	1.83%	5.35%	-185	0.94%	2.75%
5	1.11160	-89	0.46%	1.53%	-2400	12.25%	36.00%	-405	1.93%	5.84%	-184	0.88%	2.68%
6	1.12495	-102	0.49%	1.66%	-2738	13.12%	39.83%	-424	1.89%	5.89%	-174	0.78%	2.47%
7	1.13925	-112	0.49%	1.70%	-2820	12.55%	39.38%	-416	1.72%	5.52%	-155	0.65%	2.11%
8	1.15469	-117	0.47%	1.65%	-2478	10.08%	32.80%	-377	1.44%	4.76%	-124	0.48%	1.62%
9*	1.17190	-117	0.43%	1.50%	-1461	5.31 %	18.00%	-300	1.06%	3.60%	-80	0.29%	1.00%
Average	–	**79**	**0.38%**	**1.26%**	**1809**	**8.65%**	**25.99%**	**317**	**1.45%**	**4.42%**	**158**	**0.77%**	**2.26%**

- Superscript * denotes cases run with axial diffusion instead of P_3

3D Assembly Results

Case	Method	k_{eff} Diff.	Pin Powers RMS	Pin Powers Max
Average	None	2193	6.05%	10.95%
	Subplane	222	0.88%	1.64%
	Subplane+CP	114	0.45%	0.84%
	Subray-0	52	0.25%	0.54%
	Subray-1	56	0.25%	0.55%
	Subray-2	56	0.25%	0.54%
	Subray-3	56	0.25%	0.54%
Position 8	None	-91	2.88%	4.19%
	Subplane	-319	1.51%	2.66%
	Subplane + CP	-106	0.52%	0.89%
	Subray-0	-104	0.53%	0.94%
	Subray-1	-104	0.52%	0.94%
	Subray-2	-105	0.53%	0.98%
	Subray-3	-105	0.53%	0.98%

3D Assembly Results

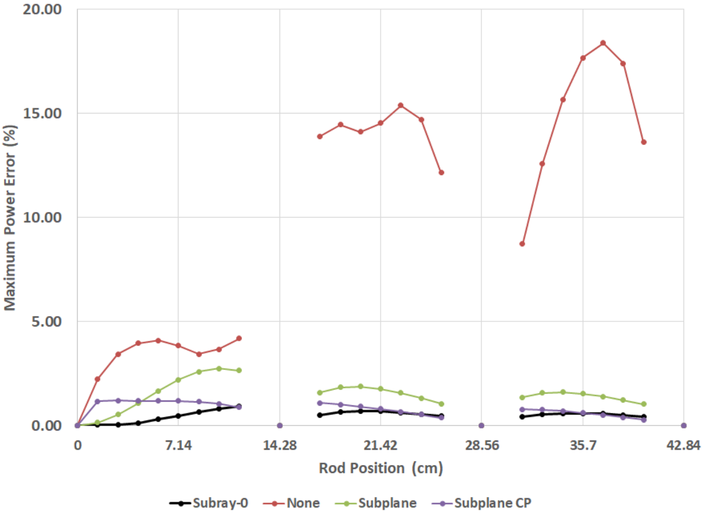

3D Core Results

Case	Method	k_{eff} Diff.	Pin Powers RMS	Max
Average	None	21	6.62%	29.30%
	Subplane	21	0.69%	3.47%
	Subplane+CP	21	0.34%	1.69%
	Subray-0	21	0.20%	1.06%
	Subray-1	25	0.20%	1.14%
	Subray-2	25	0.20%	1.11%
	Subray-3	21	0.20%	1.11%
Position 16	None	-1730	12.62%	55.69%
	Subplane	-183	1.08%	5.61%
	Subplane + CP	-76	0.45%	2.38%
	Subray-0	-46	0.30%	1.76%
	Subray-1	-54	0.35%	2.01%
	Subray-2	-53	0.34%	1.97%
	Subray-3	-53	0.34%	1.96%

3D Core Results

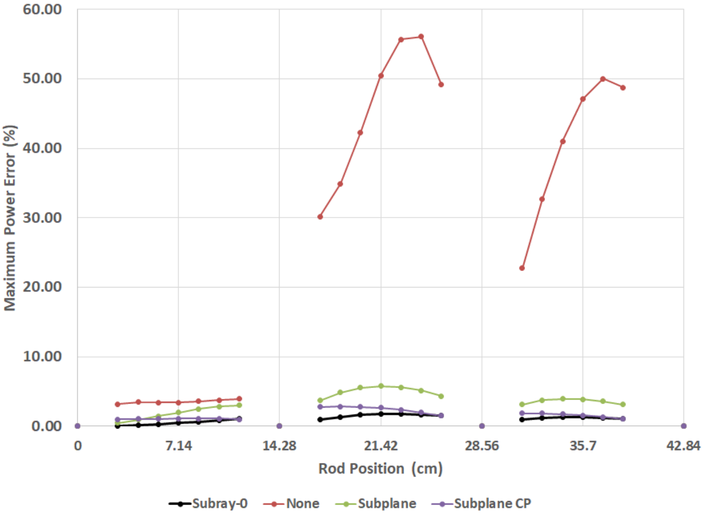

- Problem of subgrid axial heterogeneity for planar synthesis methods was described
- Rod cusping was identified as most severe axial heterogeneity
- Three new methods developed to address this problem:
  - Polynomial decusping: Fast and simple to implement, limited accuracy
  - Subplane collision probabilities: small runtime increases, good accuracy
  - Subray MOC: complicated to implement efficiently, very good acccuracy

Limitations

- Polynomial decusping:
  - Accuracy depends heavily on rod position and material
  - Generating new data for new rods can be cumbersome
- Subplane Collision Probabilities
  - Does not improve the MOC solution significantly
  - Assumes isotropic scattering
  - Neglects corner effects
- Subray MOC
  - Currently unoptimized
  - Approximations in CMFD projection/homogenization limit accuracy of source terms

Methods Improvements

- Polynomials
  - Generate data for wider variety of materials
  - Allow user input coefficients for polynomials
- Subplane collision probabilites
  - Improved load balancing
  - Other auxiliary solvers (2D R-Z CP, 2D or 3D MOC)
- Subray MOC
  - Optimization
  - Cross Section Shielding
  - Pn scattering
  - Parallelism
  - Improvements to CMFD homogenization and projection to use subregions data

Applications

- All methods could be applied to 2D/3D in addition to 2D/1D
- Apply subray MOC and subplane CP to other axial heterogeneities
  - Subplane temperature and density distributions for thermal hydraulic feedback
  - Fuel end caps, spacer grids, etc.
- Apply all methods, especially subray MOC, to a wider range of reactors

- This material is based upon work supported under an Integrated University Program Graduate Fellowship. This research was also supported by the Consortium for Advanced Simulation of Light Water Reactors under U.S. Department of Energy (DOE) contract number DE-AC05-00OR22725.
- This research made use of resources of the Oak Ridge Leadership Computing Facility, supported by the U.S. DOE under contract number DE-AC05-00OR22725; this research also made use of resources of the High Performance Computing Center at Idaho National Laboratory, supported by the U.S. DOE under contract number DE-AC07-05ID14517.
- Dr. Downar and Dr. Collins
- Committee
- MPACT/CASL team at UM and ORNL
- Family

Questions?

Multigroup Approximation

- Define multigroup flux and cross sections:

$$\varphi_g(\boldsymbol{x},\boldsymbol{\Omega})=\int_{E_n}^{E_{n-1}}\varphi(\boldsymbol{x},E,\boldsymbol{\Omega})dE \ ,$$

$$\Sigma_{x,g}\varphi_g=\int_{E_n}^{E_{n-1}}\varphi(E)\Sigma_x(E)dE\Rightarrow\Sigma_{x},g=\frac{\int_{E_n}^{E_{n-1}}\varphi(E)\Sigma_X(E) \ .dE}{\int_{E_n}^{E_{n-1}}\varphi(E)dE}$$

- Operate on steady-state transport equation by $\int_{E_n}^{E_{n-1}}(\cdot)\,dE$

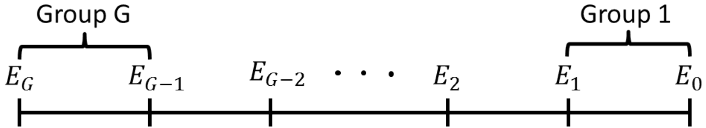

Angle Discretization

- Select a set of azimuthal and polar angles α and μ

$$\mathbf{\Omega} = \cos(\alpha)\sqrt{1-\mu^2}\boldsymbol{i} + \sin(\alpha)\sqrt{1-\mu^2}\boldsymbol{j} + \mu\boldsymbol{k}$$
$$\Rightarrow \mathbf{\Omega}_n = \cos(\alpha_n)\sqrt{1-\mu_n^2}\boldsymbol{i} + \sin(\alpha_n)\sqrt{1-\mu_n^2}\boldsymbol{j} + \mu_n\boldsymbol{k} \ .$$

- A quadrature can be used with weights w_n associated with each angle Ω_n

$$\int d\Omega = \sum_{n=1}^{N} w_n = 4\pi \ ,$$

$$\int \mathbf{\Omega} d\Omega = \sum_{n=1}^{N} \mathbf{\Omega}_n w_n = 0 \ ,$$

$$\int_{4\pi} f(\mathbf{\Omega}) d\Omega \approx \sum_{n=1}^{N} f_n w_n \ .$$

Transport-Corrected Scattering Approximation

- Modifies self-scatter and total cross-sections to account for anisotropy while performing isotropic calculations
- Neutron Leakage Conservation (NLC) Method: H-1

$$\Sigma_{s0,g\to g} = \Sigma_{s0,g\to g} + \frac{1}{3D_g} - \Sigma_{t,g}$$

- In-Scatter Method: B-11, C-12, O-16

$$\Sigma_{s0,g\to g} = \Sigma_{s0,g\to g} - \frac{1}{\phi_{1,g}} \sum_{g'=1}^{G} \Sigma_{s1,g'\to g}\phi_{1,g'}$$

- Out-Scatter Method: All other isotopes

$$\Sigma_{s0,g\to g} = \Sigma_{s0,g\to g} - \sum_{g'=1}^{G} \Sigma_{s1,g\to g'}$$

Collision Probabilities

- Used to calculate flux spectra in a pin cell
- Transport equation written so right-hand side is a single source term
  - Assumes only scattering and fission sources
  - Assumes isotropic scattering
- For 1D, pin cell is discretized into R rings, assuing flat source, flux, and cross section in each ring
- A matrix with elements $T_{g,r' \to r}$ can be determined
  - Each element is probability of neutron born in group g and region r' reaching region r
  - These probabilities are geometry-dependent, but have a general form for 1D cylindrical geometry
- Flux in each ring can be calculated from matrix $\boldsymbol{T}$, sources q, and volumes V

$$\phi_{g,r} = \sum_{r'=1}^{R} T_{g,r' \to r} q_{g,r'} V_{r'}$$

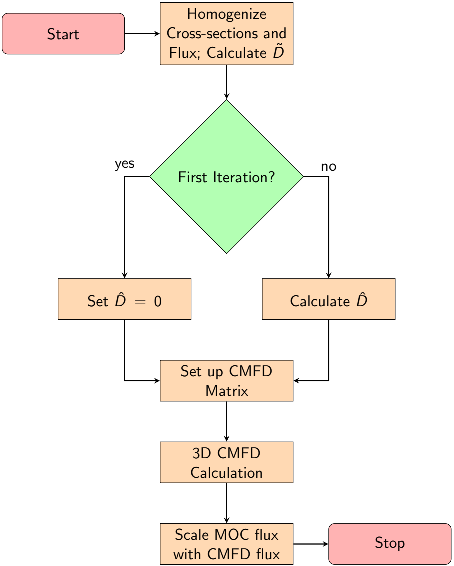
Start
Homogenize Cross-sections and Flux; Calculate $\tilde{D}$
First Iteration?
yes
no
Set $\hat{D} = 0$
Calculate $\hat{D}$
Set up CMFD Matrix
3D CMFD Calculation
Scale MOC flux with CMFD flux
Stop

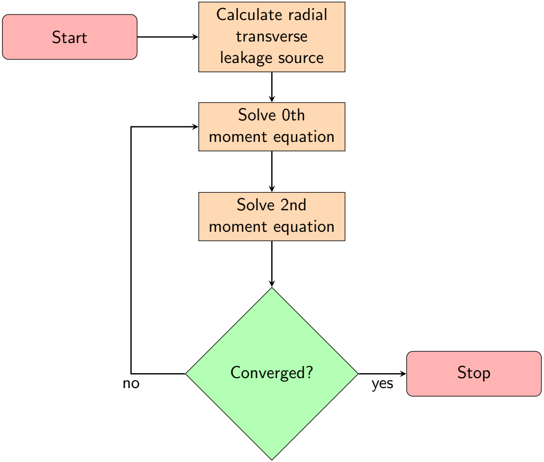
Start
Calculate radial transverse leakage source
Solve 0th moment equation
Solve 2nd moment equation
Converged?
no
yes
Stop

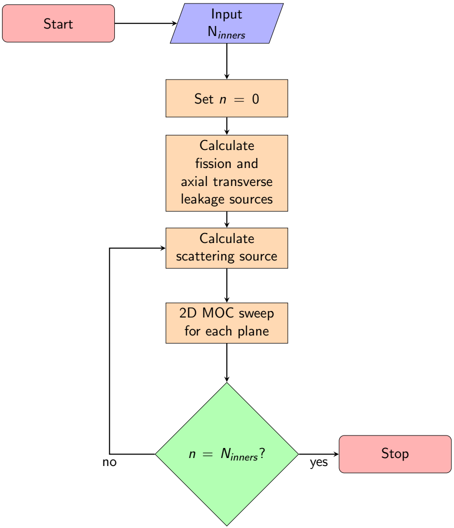
Start
Input
N_{inners}
Set $n = 0$
Calculate fission and axial transverse leakage sources
Calculate scattering source
2D MOC sweep for each plane
$n = N_{inners}$?
no
yes
Stop

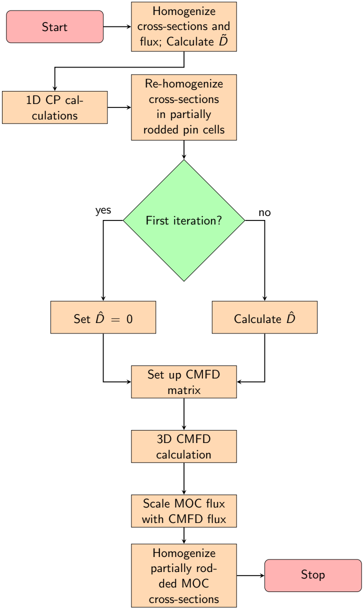
Start
Homogenize cross-sections and flux; Calculate $\tilde{D}$
1D CP calculations
Re-homogenize cross-sections in partially rodded pin cells
First iteration?
yes
no
Set $\hat{D} = 0$
Calculate $\hat{D}$
Set up CMFD matrix
3D CMFD calculation
Scale MOC flux with CMFD flux
Homogenize partially rodded MOC cross-sections
Stop

2D/3D

- 2D MOC is used to generate homogenized cross sections
- MOC planes are homogenized onto Cartesian grid
- 3D S_N is used to solve the 3D transport equation on the homogenized coarse mesh

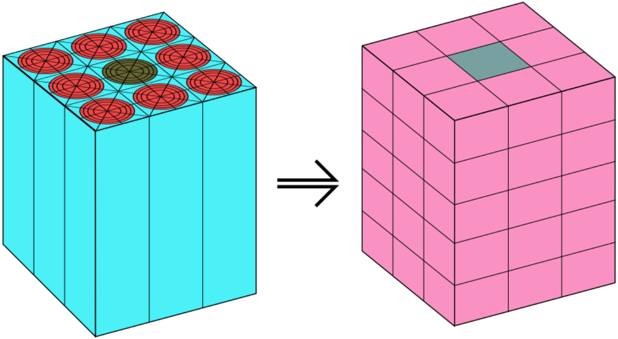

1D MOC

- 1D MOC code developed that uses MOC cross sections and slab geometry
- Fixed source and eigenvalue calculations both supported
- Analysis of angular flux behavior for cross section mixtures could be performed

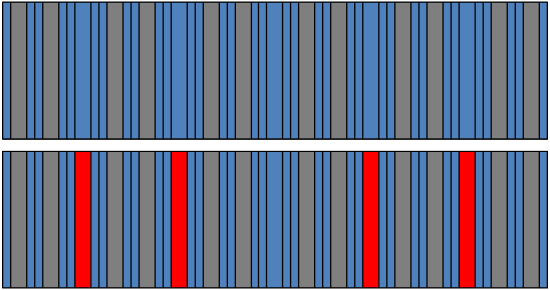

1D MOC – Fixed Total Source

- Scalar flux, group 7

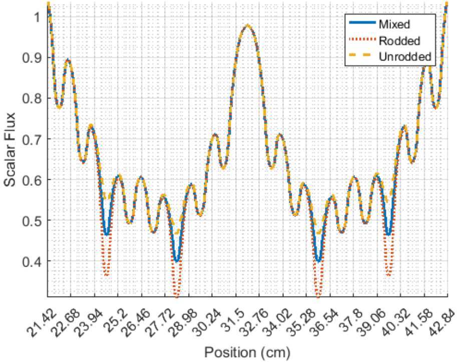

1D MOC – Fixed Total Source

- Rightgoing angular flux, group 1 (left) and 7 (right)

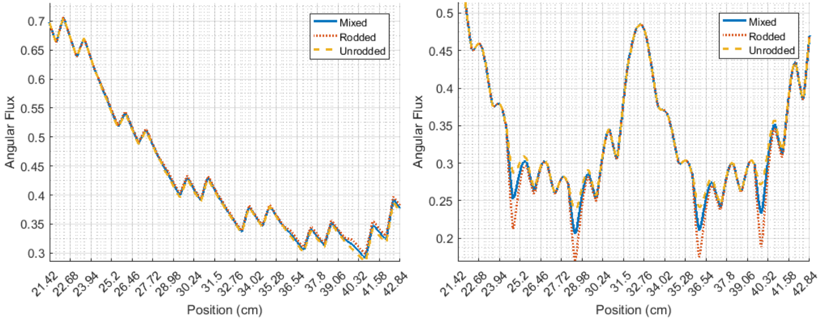

1D MOC – Fixed Fission Source

- Rightgoing angular flux, group 1 (left) and 7 (right)

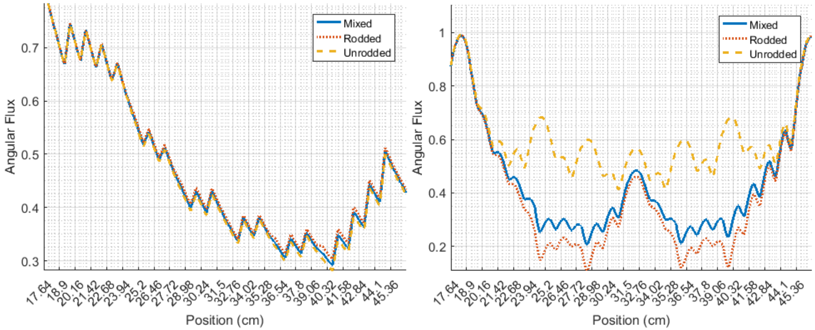

1D Subray MOC

- 1D MOC code developed that uses MOC cross sections and slab geometry
- Fixed source and eigenvalue calculations both supported
- Allowed for a prototype of subray MOC concept

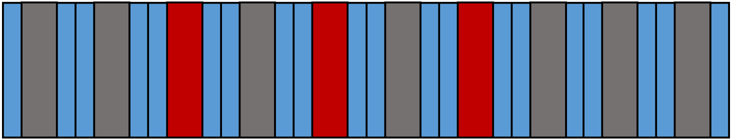

1D Subray MOC

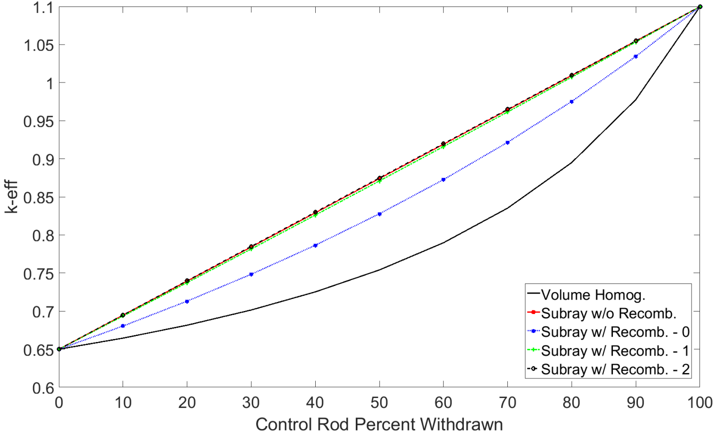

1D Subray MOC

- 50% rodded, scalar flux, group 1

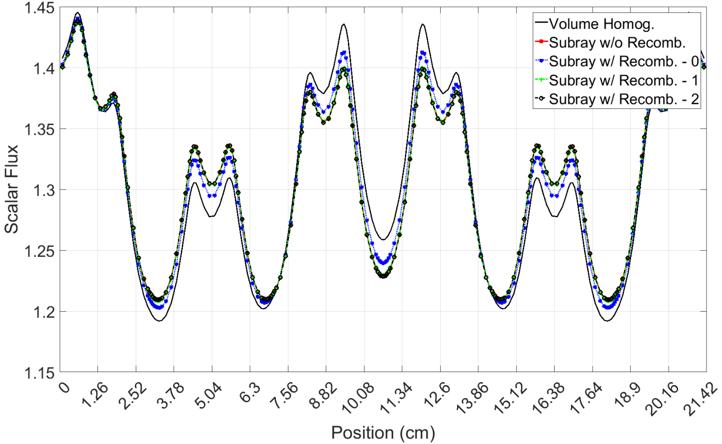

1D Subray MOC

- 50% rodded, scalar flux, group 7

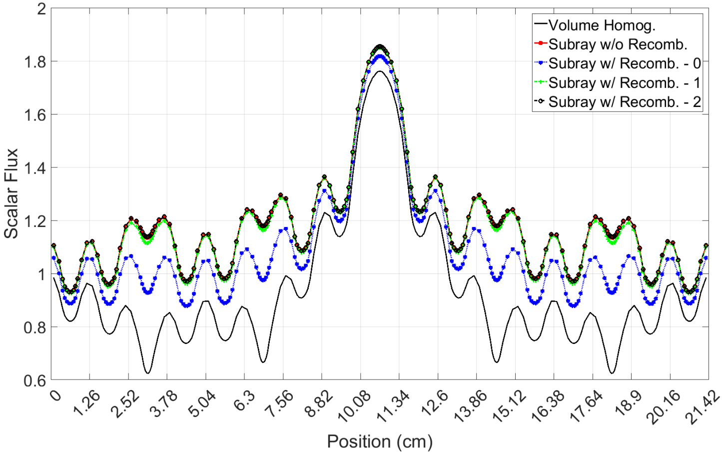

J. Y. Cho *et al.*
"Three-dimensional heterogeneous whole core transport calculations employing planar moc solutions."
In: *Trans. Am. Nucl. Soc.*, volume 87, (pp. 234–236) (2002).

M. Hursin, B. Kochunas, and T. Downar.
DeCART Theory Manual.
Technical report, University of Michigan (2008).

H. G. Joo *et al.*
"Methods and performance of a three-dimensional whole-core transport code decart."
In: *PHYSOR 2004 – The Physics of Fuel Cycles and Advanced Nuclear Systems: Global Developments*. Chicago, Illinois (2004).

MPACT Team.
MPACT Theory Manual.
Technical report, Oak Ridge National Laboratory and the University of Michigan (2015).

K. Smith.
"Nodal method storage reduction by nonlinear iteration."
Trans. Am. Nucl. Soc., **44**: p. 265 (1983).

R. G. McClarren.
"Theoretical aspects of the simplified pn equations."
Transport Theory and Statistical Physics, **39(2-4)**: pp. 73–109 (2011).

H. Finnemann, F. Bennewitz, and M. Wagner.
"Interface current techniques for multidimensional reactor calculations."
Atomkernenergie, **30(2)**: pp. 123–128 (1977).

J. Askew.
A characteristics formulation of the neutron transport equation in complicated geometries.
Technical report, United Kingdom Atomic Energy Authority (1972).

M. Halsall.
CACTUS, a characteristics solution to the neutron transport equations in complicated geometries.
Technical report, UKAEA Atomic Energy Establishment (1980).

B. Cho and N. Z. Cho.
"A nonoverlapping local/global iterative method with 2-d/1-d fusion transport kernel and p-cmfd wrapper for transient reactor analysis."
Annals of Nuclear Energy, **85**: pp. 937–957 (2015).

Y. S. Jung and H. G. Joo.
"Control rod decusping treatment based on local 3-d cmfd calculation for direct whole core transport solvers."
In: *Proceedings of the International Congress on Advances in Nuclear Power Plants (ICAPP)* (2014).

J. C. Gehin.
A quasi-static polynomial nodal method for nuclear reactor analysis.

Technical report, Oak Ridge Inst. for Science and Education, TN (United States); Massachusetts Inst. of Tech., Cambridge, MA (United States) (1992).

M. Ryu and H. G. Joo.
"ntracer whole core transport solutions to c5g7-td benchmark."
In: *Proceedings of the International Conference on Mathematics and Computation (M&C 2017)*. Jeju, Korea (2017).

A. M. Graham, B. S. Collins, and T. Downar.
"Improvement of the 2d/1d method using the sub-plane scheme."
In: *Proceedings of the International Conference on Mathematics and Computation (M&C 2017)*. Jeju, Korea (2017).

A. M. Graham, B. S. Collins, and T. Downar.
"Rod decusping techniques for the 2d/1d method."
In: *Proceedings of the International Conference on Mathematics and Computation (M&C 2017)*. Jeju, Korea (2017).

A. T. Godfrey.
VERA Core Physics Benchmark Progression Problem Specifications.
Technical report, Oak Ridge National Laboratory.
URL http://www.casl.gov/docs/CASL-U-2012-0131-004.pdf
(2014).

E. E. Lewis *et al.*
Benchmark on Deterministic Transport Calculations without Spatial Homogenization.
Technical report, Nuclear Energy Agency Organisation for Economic Cooperation and Development (NEA-OECD) (2003).

E. E. Lewis *et al.*
Benchmark on Deterministic Transport Calculations without Spatial Homogenization: MOX Fuel Assembly 3-D Extension Case.
Technical report, Nuclear Energy Agency Organisation for Economic Cooperation and Development (NEA-OECD) (2005).